

Tuned liquid column dampers in offshore wind turbines for structural control

Shane Colwell, Biswajit Basu*

Department of Civil, Structural and Environmental Engineering, Trinity College Dublin, Ireland

ARTICLE INFO

Article history:

Received 19 June 2007

Received in revised form

20 July 2008

Accepted 1 September 2008

Available online 1 October 2008

Keywords:

TLCD

Offshore wind turbine

Vibration control

Wind loading

Wave loading

Correlation

ABSTRACT

With offshore wind turbines becoming larger, being moved out further at sea and subjected to ever greater wind and wave forces, it is necessary to analyse the dynamics and minimise the responses of these structures. In this paper, the structural responses of offshore wind turbines are simulated with an attached damper (Tuned Liquid Column Damper (TLCD)) for controlling the vibrations induced within the structure. This requires a realistic simulation of the forces that these tall, flexible and slender structures are subjected to, and consequently the implementation of a damper to control the resulting undesirable vibrations that are induced within the structure. Since sea waves are caused by wind blowing for a sufficiently long time, the state of the sea is related to wind parameters and there exists the possibility of correlating wind and wave loading conditions on structures. The Kaimal spectrum for wind loading is combined with the JONSWAP wave spectrum to formulate correlated wind and wave loadings. The offshore turbine tower is modelled as a Multi-Degree-of-Freedom (MDOF) structure. Cases for flat sea conditions, with which parallels to onshore wind turbines may be drawn, are first simulated. Simulations are presented for the MDOF structure subjected to both 'moderate' and 'strong' wind and wave loadings. Cases of the blades lumped at the nacelle along with rotating blades are investigated. The reduction in bending moments and structural displacement response with TLCDs for each case are examined. A fatigue analysis is carried out and the implementation of TLCDs is seen to enhance the fatigue life of the structure. An analysis, taking into account the extended fatigue life and reduced bending moments on the structure-TLCD system, is presented.

© 2008 Elsevier Ltd. All rights reserved.

1. Introduction

With the present day energy crisis becoming more pronounced, due to depletion of fossil fuel stocks, offshore wind turbines are becoming a viable and attractive means of producing electricity. An offshore wind turbine harnesses the wind energy out at sea to produce electrical energy. To dynamically examine these slender structures in an offshore environment, it is necessary to correlate wind and wave loadings, and to investigate the force-structure interaction arising from such a correlation. Due to the slenderness of offshore wind turbines, the combination of wind and wave forces may produce excessive vibrations that will inhibit the mechanical system in the nacelle from converting wind energy to electrical energy. Reductions in fatigue life, and higher foundation and tower construction costs will also arise from uncontrolled vibrations in the offshore wind turbine structural system.

Turbulence from offshore wind produces small capillary waves at the sea surface, with similarly small wavelengths in the range of centimetres. The wind acts on the tiny walls that these ripples create, causing them to become larger. Wind blowing over the

wave produces pressure differences along the wave profile, causing the wave to grow. The process is unstable because, as the wave gets bigger, the pressure differences get bigger, and the wave grows exponentially. Finally, the waves begin to interact among themselves to produce longer waves [1]. The interaction transfers wave energy from short waves generated by the Miles mechanism, to waves with frequencies slightly lower than the frequency of waves at the peak of the spectrum. Eventually, this leads to waves going faster than the wind, as noted by [2].

Davenport [3] proposed an expression for the velocity spectrum for the distribution of energy within turbulent wind flow, at a height related to the size of gusts at that height. However, this spectrum was independent of height, and was also seen to overestimate the energy in the higher frequency range. Harris [4] proposed a velocity spectrum which was independent of height, and that guaranteed a non-zero integral length scale of turbulence. Harris [5] subsequently provided a wind spectrum based on a modified version of the Von-Kármán spectrum, which included the variation of spectral energy with height. Kaimal et al. [6] developed the first expression for the variation of spectral energy with height, which includes eddy currents of varying size acting between the structural nodes.

Despite the irregular random nature of wind inducing seemingly random wave heights and wave periods in a typical offshore

* Corresponding author.

E-mail address: basub@tcd.ie (B. Basu).

setting, any associated changes that occur with the state of the sea are slow enough to allow the characterization of a sea state. A sea state is defined [7] as a wave situation that is approximately constant during some time interval of appropriate duration characterized by the significant wave height H_s and the characteristic zero crossing point T_z . The wave height H_s is the average height (trough to crest) of the one-third highest waves valid for the indicated 12 h period. The sea surface, which is made up of a superposition of sinusoidal waves with random heights and periods, will oscillate vertically in an aperiodic manner around a zero level reference point. The time intervals between each meeting of the sea surface and the zero level vary around an average value, T_z . Hence, the process is narrow-banded, and can be related to the mean wind speed.

Pierson and Moskowitz [2] assumed that if the wind blew for a long time over a large area, the waves would come into equilibrium with the wind, and low frequency waves are developed in a fully developed sea. A large area being defined as 5000 wave lengths on a side, and a long time being defined as 10,000 wave periods [8]. This is the concept of a fully developed sea. To obtain a spectrum of a fully developed sea, they used accelerometers to measure wave data on ships in the North Atlantic. Hasselmann et al. [9] measured wave data in the North sea and discovered that a sea never actually becomes fully developed. They developed their own spectrum (JONSWAP), which takes into account a higher peak than the Pierson–Moskowitz spectrum.

The expression for the in-line force per unit length along a cylinder was first investigated over 50 years ago [10]. The mitigation of vibrations of an offshore structural system with an additional damper, when subjected to in-line random wave forces, was investigated [11]. In the stochastic analysis performed, a random type of wave force derived from the Morison equation for small bodies was applied. It was observed that, in terms of the power spectral density, the effect of the vibration mitigation and the dynamic performance of the offshore structural system were greatly improved when the new damping devices were applied to the offshore structural system. By considering the environmental loading on a structure with TMD to be a long-term nonstationary stochastic process, characterized by a probabilistic power spectral density function (PSDF) [12], it was found that the use of a TMD could significantly reduce the fatigue damage of an offshore structure. A method of determining the ‘generalized’ wave force was based on an analytical approximation of the mode shape function, together with the physical wave loading being calculated from linearized Morison equation [13]. The effectiveness of H_2 active control is numerically demonstrated, with a reduction in the standard deviation of the deck motion of passive TMD case of 50% for the active TMD case with H_2 active control. A jacket-type offshore platform modelled as a SDOF structure with attached active mass damper (AMD) was recently simulated by using the linearized Morison equation is used to estimate the wave load [14]. An active control strategy [15] was used to determine the control force magnitude for serviceability and survival of tension leg platforms (TLPs), subjected to wind and wave loadings. Significant reduction in low-frequency hull motion of the TLP was observed. Thus, although several investigations have been carried out for the control of offshore structures, little attention has been focused on the vibration control of flexible offshore structures subjected to joint wind and wave loading with an additional damping system.

Structural engineers are increasingly turning to additional damping systems to protect structures from the damaging effects of the environment. Tuned liquid dampers (TLD), of which Sakai et al. [16] proposed the first tuned liquid column damper (TLCD) as a means of suppressing vibrations within structures, are dampers whose damping effects depend on a liquid residing in the damper and which are specifically tuned to the natural frequency of

a structure. TLCDs, which are U-shaped liquid dampers, are a variation on the TLD which aim to utilize the gravitational restoring force of the displaced liquid more efficiently. The frequency of oscillation of the liquid in a TLCD for vibration control is specifically tuned to the natural frequency of a structure. The tuning ratio, which is the ratio of the natural frequency of the TLCD to that of the structure, is optimised in order to ensure an efficient transfer of shear force from the TLCD to the structure. Vibrations are suppressed within a structure with an attached TLCD, due to the gravitational restoring force acting on the displaced liquid. It is possible that a non-optimal design of the TLCD would result in dead mass in the TLCD, which does not present a problem in a TLD. However, in a TLCD energy is also dissipated through orifice(s) which reside within the cross section of the damper. The utilization of TLCDs as a means of suppressing vibration energy within structures is being accelerated due to factors such as: they can dissipate very low amplitude excitations (unlike Tuned Mass Dampers (TMDs)), they are consistent over a wide range of excitation levels, and they are self-contained passive damping devices, with little auxiliary equipment, personnel or power required to operate and maintain it, and are easy to install. TLCDs typically comprise of 1%–2% of the total mass of the structure, compared with 4%–5% of that with a pendulum type damper. Compared with other liquid dampers (e.g., Tuned Liquid Dampers), TLCDs prove more efficient with respect to volumetric efficiency (when adequate horizontal space is available), TLCDs introduce extra damping effects and variable damping due to the orifice, and the damping effect of TLCDs is easier to quantify. Changing soil properties over time may alter the natural frequencies of the structure, and although the TLCD is usually tuned to the natural frequency of the structure, the orifice damping present in the TLCD will also dampen the shifted frequencies to a certain extent.

TLCDs have been implemented in Hotel Cosima, Hyatt Hotel and Ichida Building in Osaka [17] and also in One Wall Centre in Vancouver. An investigation into the effects of liquid storage tanks containing glycol on the dynamic response of offshore structures concluded that prudent selection of the geometry of the storage tanks would dampen the response of the platform of the offshore structure [18]. Samali et al. [19] investigated the application of TLCDs to tall buildings, and concluded that they may be successfully used to damp vibrations in such buildings. Xu et al. [20] studied the application of TLCDs compared to TMDs and concluded that TLCDs are as effective as TMDs in damping structures, but also possess practical advantages. Hochrainer [21] established a geometric analogy between the sealed TLCD (linearized) with the gas-spring effect (in parallel action with the gravitational restoring force) to the linear TMD (pendulum type). Balendra et al. [22] demonstrated the effectiveness of TLCDs in suppressing wind-induced accelerations for towers with varying natural frequencies. Balendra et al. [23] studied the performance of the TLCD on vibration control of structures with a varying degree of taper. They concluded that flexural buildings experienced greater acceleration and displacement reductions than shear buildings. They also observed that the height at which the maximum reduction in structural acceleration is achieved, decreases with the degree of taper. Gao et al. [24] investigated the optimisation of the TLCD through a parametric study. It was seen that it is possible to install a TLCD in a flexible structure by increasing the area ratio when the required length of liquid column is too long. Hochrainer and Ziegler [25] presented optimal solutions for benchmark MDOF structures with multiple TLCD. Ziegler [26] showed that the TLCD is a practical and cost effective alternative to the TMD in civil engineering structures. Ghosh and Basu [27] proposed and studied the use of a compliant spring connected TLCD for nonlinear structures. Other studies into TLCDs have been conducted by [28–36].

In general, TLCDs prove more volumetrically efficient than TLDs when appropriate horizontal space is available. In the design of an offshore wind turbine with equipped TLCD, provision would have to be made to facilitate the horizontal liquid length. While implementing a TLCD in an offshore wind turbine, provision also must be made to accommodate the TLCD. A provision for accommodating TLCDs in a wind turbine has been recently presented [37], however other various placements of the TLCD, with varying parameters, are realisable in offshore wind turbines by accommodating the TLCD in/on the nacelle or in the tower. It may so happen, that for a possible installation of TLCD in wind turbines, the efficiency may have to be sacrificed to a certain extent, due to the lack of availability of ‘horizontal length’ even though the optimal tuning criterion may be met.

By implementing TLCDs in offshore wind turbines [38], the vibrations and the bending moments are expected to be reduced, and hence there will be an increase in the fatigue life of the structure [39]. The DNV offshore standards [40] calculate the fatigue life under the assumption of linearly cumulative damage. A case study of fatigue analysis of an offshore wind power generation facility subjected to wind and wave loading was recently carried out [41]. The wave spectrum was modelled by the Pierson–Moskowitz spectrum, and the fluctuating wind speed time history was prepared using the Ochi–Shin spectrum. They used the rain-flow calculation method and the zero-upcrossing calculation method to estimate the fatigue life at various points of an offshore wind turbine assembly subjected to wind and wave loading. In a case such as an offshore wind turbine tower, where the stress fluctuations caused by wind and wave excitations are superimposed, it can be used as a suitable calculation method.

In this paper, the Kaimal spectrum for a wind excitation is combined with the JONSWAP wave spectrum to excite the offshore wind turbine. By exciting an offshore wind turbine tower modelled as a MDOF system, using joint wind and wave loadings, the dynamic response of the turbine tower is controlled using TLCDs, which can be accommodated within the available horizontal length in the wind turbine tower/nacelle. The offshore wind turbine is excited for cases with and without the TLCD for the purpose of comparison. Cases for turbine blades lumped at the nacelle and rotating blades are simulated, to investigate the effects of the rotation of blades. It is shown that implementing TLCDs will decrease the structural costs, and prolong the life of the tower. The fatigue life calculation for the tower is carried out using the rain-flow counting technique for cases with and without TLCD. In addition, when the dynamic response of the turbine is such as to shut down the harnessing of the wind’s energy, the addition of a TLCD will reduce the dynamic response of the tower, and hence increase the reliability of the production of energy.

2. MDOF Offshore wind turbine structure with TLCD

The TLCD considered is composed of a U-shaped pipe with orifice installed in it. The equation of motion of the TLCD for the structure-TLCD system as developed by [16], is given as

$$\rho AL\ddot{u} + \frac{1}{2}\rho A\xi |\dot{u}| \dot{u} + 2\rho Agu = -\rho AB \{ \ddot{x}_n \} \quad (1)$$

where, u is the change in elevation of the liquid column, A is the cross sectional area of the TLCD, B is the horizontal dimension, L is the length of the liquid column and x_n is the horizontal displacement at the top of the structure where the TLCD is installed. The overdot represents differentiation with respect to time. The notations ξ , ρ and g represent non-linear coefficient of head loss, controlled by the opening ratio of the orifice (ratio of the diameter of the orifice to that of the horizontal tube), liquid

mass density and the acceleration due to gravity respectively. Normalizing Eq. (1) with respect to the mass of the liquid yields

$$\ddot{u} + \frac{\xi}{2L} |\dot{u}| \dot{u} + \omega_L^2 u = -\alpha \{ \ddot{x}_n \} \quad (2)$$

where $\alpha (= B/L)$ is the ratio of the horizontal portion of the TLCD tube to its total length and $\omega_L = \sqrt{2g/L}$ is the natural circular frequency of the TLCD.

2.1. MDOF offshore turbine with blades lumped at the nacelle

The case where the mass of the blades is concentrated into the nacelle is first examined. The equation of motion for the structural model, which is represented as an n -degree of freedom structure (Fig. 1), with attached TLCD is given by

$$M\ddot{X} + C\dot{X} + KX = P(t) - \rho AB\ddot{u}R_1 - \rho AL\ddot{x}_n R_1 \quad (3)$$

where $X = \{x_1, x_2, \dots, x_n\}$ denotes the n -dimensional horizontal displacement vector of the structure and \ddot{x}_n represents the horizontal acceleration at top of the tower (base of the TLCD container); M , C and K are the n -dimensional mass, damping and stiffness matrices of the structure, respectively; $P(t)$ is the n -dimensional total force vector and $R_1 = \{1, 0, \dots, 0\}^\top$ is an n -dimensional constant vector. The MDOF representation of the wind turbine has been used before [42] to study the structural dynamics of offshore wind turbines subjected to extreme wind loading. In Fig. 1, the virtual mass of the underwater components are taken into account. The last two terms on the right of Eq. (3) represent the force transmitted from the TLCD into the structure.

The structural displacement response can be represented as a product of the mode shape matrix, Φ , normalized with respect to the structural mass matrix and the n -dimensional modal coordinate vector, η . By inserting $X = \Phi\chi$ into Eq. (3), the governing equation of the system becomes

$$I_m \ddot{\chi} + \Theta \dot{\chi} + \Gamma \chi = \phi^T P(t) - \rho AB\phi^T \ddot{u} R_1 \quad (4)$$

where the n -dimensional diagonal matrices $\Theta = \phi^T C \phi = \text{diag}(2\xi_1\omega_1, 2\xi_2\omega_2, \dots, 2\xi_n\omega_n)$, $\Gamma = \phi^T K \phi = \text{diag}(\omega_1^2, \omega_2^2, \dots, \omega_n^2)$ and I_m is an n -dimensional matrix. The terms ξ_i and ω_i represent the damping ratio and natural frequency of the i th mode respectively. The ratio of the mass of the liquid in the damper to that of the structure is given by $\mu (= \rho AL/\text{trace}(M))$ and the n -dimensional nodal coordinate where the structure is connected to the TLCD is given by x_n .

By combining Eqs. (2) and (4), the following equation for the wind turbine idealized as a MDOF with a lumped mass of the blades at the free end and incorporating TLCD is obtained as

$$M_{\text{mod}} \ddot{Z} + C_{\text{mod}} \dot{Z} + K_{\text{mod}} Z = F_T(t) \quad (5)$$

in which the the $(n+1)$ -dimensional displacement vector Z , the $(n+1)$ -dimensional generalized mass matrix M_{mod} , damping matrix C_{mod} and stiffness matrix K_{mod} , and the $(n+1)$ dimensional generalized total input force vector F_T , are given by

$$Z = \begin{Bmatrix} \chi \\ u \end{Bmatrix}, \quad (6)$$

$$M_{\text{mod}} = \begin{bmatrix} I_m & \text{trace}(M)\mu\alpha\phi^T R_1 \\ \alpha R_1^T \phi & 1 \end{bmatrix}, \quad (7)$$

$$C_{\text{mod}} = \begin{bmatrix} \Theta & 0 \\ 0 & \frac{\xi}{2L} |\dot{u}| \end{bmatrix}, \quad (8)$$

$$K_{\text{mod}} = \begin{bmatrix} \Gamma & 0 \\ 0 & \omega_L^2 \end{bmatrix}, \quad (9)$$

$$F_T = \begin{Bmatrix} \phi^T P \\ 0 \end{Bmatrix} \quad (10)$$

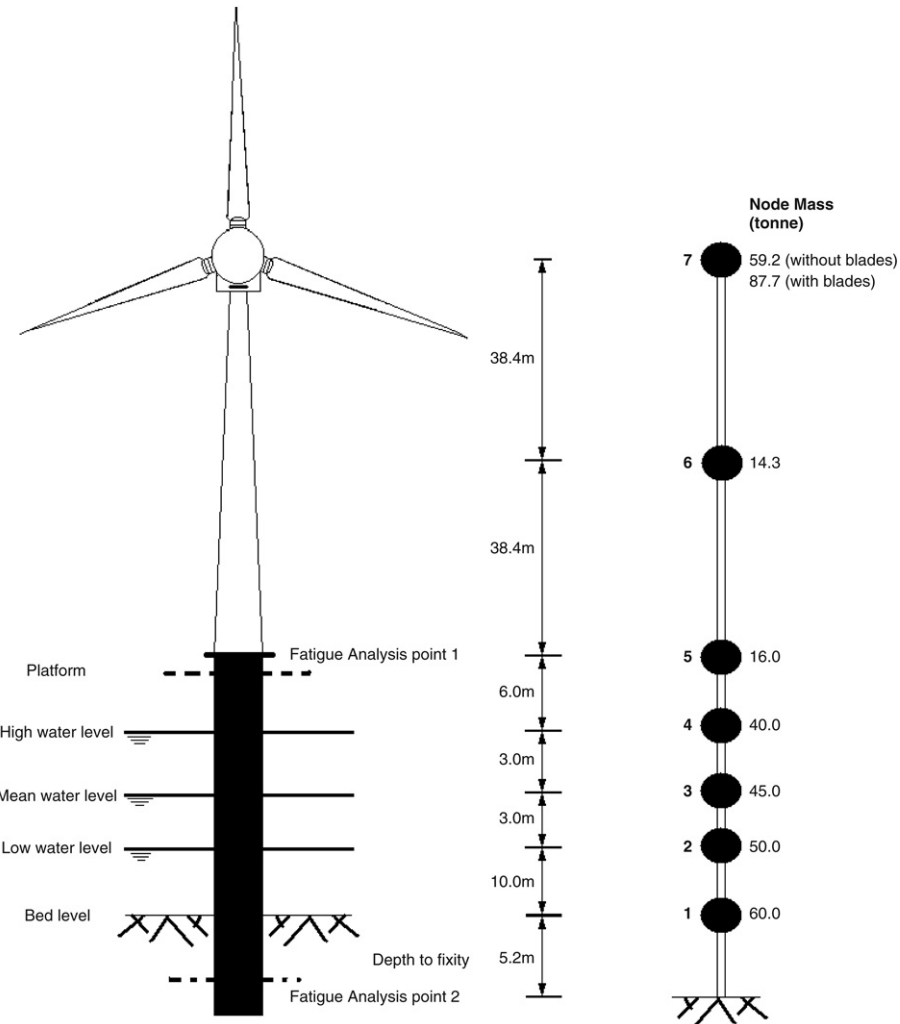


Fig. 1. Structural model.

3. Wind excitation

The wind loading on any structural member is decomposed into a constant mean wind load, and a fluctuating wind component. The total wind force on any structural member is a summation of the mean and the fluctuating components. For wind excitations, the PSD matrix, $S_{vv}(\omega)$ is obtained from the along wind excitation applied to the structure and the turbulence between two points for a N degree of freedom (DOF) structure. The spectrum used in this paper to simulate the fluctuating along wind velocity spectrum was proposed by [6]

$$S_{vv}(z, \omega) = \frac{v_*^2}{2\pi\omega} \frac{200n_m}{(1 + 50n_m)^{5/3}} \quad (11)$$

in which

$$n_m = \frac{2\pi\omega z}{\bar{v}(z)} \quad (12)$$

and

$$\bar{v}(z) = \frac{1}{k_{vk}} v_* \ln \frac{z}{z_0} \quad (13)$$

with z being the vertical coordinate, ω is the frequency (rad/s), v_* is the friction velocity (m/s), n_m is the Monin coordinate, k_{vk} is the Von-kármán's constant and z_0 is the roughness length. When a continuous structure is discretised into a MDOF system, the modal

fluctuating drag force power spectrum, which includes spatial correlation information, is expressed as

$$S_{f_{D,Mj}}(\omega) = (C_D A_T \rho)^2 \sum_{k=1}^N \sum_{l=1}^N S_{V_k V_l}(\omega) \bar{v}_k \bar{v}_l \phi_{T,j}(k) \phi_{T,j}(l) \quad (14)$$

where, A_T is the total area of the structure exposed to the wind, ' k ' and ' l ' are spatial nodes, $S_{V_k V_l}(\omega)$ is the velocity auto PSD when $k = l$ and the cross PSD when $k \neq l$, \bar{v}_k and \bar{v}_l are the mean wind velocities at nodes k and l respectively, and $\phi_{T,j}(k)$ and $\phi_{T,j}(l)$ are the nodal k and l components of the ' j 'th mode shape. The auto and cross PSD terms is given as

$$S_{V_k V_l}(\omega) = \sqrt{S_{V_k V_k}(\omega) S_{V_l V_l}(\omega)} \text{coh}(k, l; \omega) \quad (15)$$

where, $S_{V_k V_k}(\omega)$ and $S_{V_l V_l}(\omega)$ are the velocity auto PSDs at nodes k and l respectively. The spatial coherence function between nodes k and l is given by [43]

$$\text{coh}(k, l; f) = \exp \left(-\frac{|k - l|}{L_s} \right) \quad (16)$$

where, $|k - l|$ is the spatial separation and L_s is the length scale given by

$$L_s = \frac{\hat{v}}{2\pi\omega D}. \quad (17)$$

In Eq. (17) \hat{v} is the average mean wind velocity between nodes k and l and D is a decay constant. Any arbitrary fluctuating drag force time-history, $f_{D,Mj}(t)$, with zero mean, may be represented by a discrete Fourier series with a discretised version of a continuous frequency content as

$$f_{D,Mj}(t) = \sum_{k=1}^{\infty} a_k \cos(\omega_k t) + \sum_{k=1}^{\infty} b_k \sin(\omega_k t) \quad (18)$$

where a_k and b_k are the Fourier coefficients, ω_k is the discretised frequency and t is the time instant. Assuming the fundamental mode contributes significantly to the response of the tower (with $j = 1$), the total drag force experienced is made up of a mean component and a fluctuating component

$$F(t) = \bar{f}_{\text{mean},i} + f_{D,M1}(t). \quad (19)$$

The mean drag force at node 'i' can be represented as

$$\bar{f}_{\text{mean},i} = \frac{1}{2} C_D A_i \rho \bar{v}_i^2 \quad (20)$$

where, C_D , A_i , ρ and \bar{v}_i are the drag coefficient, area associated with node 'i', air density and mean wind velocity at node i , respectively. The total drag forces can be applied at different nodes on the tower.

3.1. Wind excitation on rotating blades and coupled blade/tower system

The rotating wind turbine blades are modelled as discretised versions of prismatic cantilevered beams of rectangular hollow cross section. The variation of the mean velocity with rotating blades is expressed as

$$\bar{v}_i = \bar{v}_i(H) + \bar{v}_{i,\text{ref}} \cos(\Omega t) \quad (21)$$

where, $\bar{v}_i(H)$ and $\bar{v}_{i,\text{ref}}$ are the mean wind velocity at the respective node height and the varying component of the wind velocity, respectively. Using Eq. (21) in Eq. (20), the mean nodal drag force is calculated. In the case of the rotating blades, the fluctuating nodal drag force is given by

$$f'_i(t) = C_D A_i \rho \bar{v}_i v'_i(t) \quad (22)$$

where, $v'_i(t)$ is the fluctuating velocity component described by Eq. (11). The total force at node i is obtained from the summation of the mean and fluctuating nodal drag forces.

The effective shear force transmitted into the nacelle of the tower due to blade vibration may be given by [44]

$$V'_{bl}(t) = V_{bl}(t) + \ddot{x}_n(t) M_{bl,t} \quad (23)$$

where $M_{bl,t}$ is the mass of the three blades and $\ddot{x}_n(t)$ is the absolute acceleration at the nacelle of the tower. The total base shear, $V_{bl}(t)$, exerted by a rotating blade is equal to the summation of the inertial forces over the entire length of the blade

$$V_{bl}(t) = \bar{m}_b \int_0^{L_b} \{\ddot{u}_b(t)\} dx \quad (24)$$

where \bar{m}_b is the mass per unit length of the blade, L_b is the length of the blade and acceleration of the blade is, $\ddot{u}_b(t)$, relative to the nacelle. To account for the effect of rotating blades on the response of the tower, a sub-structure approach is followed [45]. The response of the rotating blades subjected to wind loading is calculated at first. Then, the coupling of the blades and the tower is accounted for, by assuming the effect of the motion at the top of the tower and transfer of shear from the blades to the top of the tower (nacelle).

4. Wave excitation

Data was collected [1] and analysed during the Joint North Sea Wave Observation Project (JONSWAP) and it was found that the wave spectrum continues to develop through non-linear, wave-wave interactions, even for very long times and distances compared with the Pierson–Moskowitz spectrum. The JONSWAP spectrum takes into account the higher peak of the spectrum in a storm for the same total energy as compared with Pierson–Moskowitz and also the occurrence of frequency shift of the spectra maximum. The spectrum takes the form

$$S_{\eta\eta}(\omega) = \frac{\alpha g^2}{\omega^5} \exp\left[-\frac{5}{4}\left(\frac{\bar{\omega}_m}{\omega}\right)^4\right] \gamma \exp\left[\frac{(\omega-\bar{\omega}_m)^2}{2\sigma^2\bar{\omega}_m^2}\right] \quad (25)$$

where, η is the function of water surface elevation. Eq. (25) defines a stationary Gaussian process of standard deviation equal to 1. In Eq. (25), γ is the peak enhancement factor (3.3 for the North sea), g is the acceleration of gravity and ω is the circular wave frequency. The wave data from the JONSWAP project was used to calculate the values of the constants in Eq. (25) as follows

$$\alpha = 0.076 \left(\frac{U_{10}^2}{Fg}\right)^{0.22}, \quad (26)$$

$$\bar{\omega}_m = 22 \left(\frac{g^2}{U_{10} F}\right)^{1/3}, \quad (27)$$

and

$$\sigma = \begin{cases} 0.07 & \omega \leq \bar{\omega}_m \\ 0.09 & \omega > \bar{\omega}_m \end{cases} \quad (28)$$

where U_{10} is the mean wind speed 10 m from the sea surface, F (fetch) is the uninterrupted distance over which the wind blows (measured in the direction of the wind) without a significant change of direction. The fetch varies in its non-dimensional form as follows [7]

$$10^{-1} < \frac{gF}{U_{10}^2} < 10^4. \quad (29)$$

The total wave force acting on the offshore wind turbine is

$$f_w(t) = \int_0^d p(z, t) \phi_w(z) dz \quad (30)$$

where, $\phi_w(z)$ is the shape function of the offshore structure exposed to the wave loading, d is the depth of the water surface, z is the vertical coordinate axis, $p(z, t)$ is the wave force acting on the column that can be calculated by the linearized Morison equation [46]

$$p(z, t) = K_d \sqrt{\frac{8}{\pi}} \sigma_v v(z, t) + K_m a(z, t) \quad (31)$$

with,

$$K_d = (1/2) C_d \rho d_e, \quad (32)$$

$$K_m = (1/4) C_m \rho \pi d_e^2 \quad (33)$$

and C_d is the drag coefficient, C_m is the inertia coefficient, d_e is the equivalent characteristic diameter of the turbine monopole and ρ is the fluid density. Following the linear wave theory, the horizontal velocity $v(z, t)$ and acceleration $a(z, t)$ of the water particle are both functions of the wave elevation [13]

$$v(z, t) = \omega \frac{\cosh(kz)}{\sinh(kd)} \eta(t) \quad (34)$$

$$a(z, t) = -j\omega^2 \frac{\cosh(kz)}{\sinh(kd)} \eta(t) \quad (35)$$

where k is the wave number that can be determined from the linear dispersion relationship

$$\omega^2 = gk \tanh(kd). \quad (36)$$

The standard deviation of the velocity at location z can be obtained as

$$\sigma_v = \left[\int_0^\omega |T_v|^2 S_{\eta\eta}(\omega) d\omega \right]^{1/2} \quad (37)$$

in which

$$T_v = \omega \frac{\cosh(kz)}{\sinh(kd)}. \quad (38)$$

Substituting the appropriate terms into Eq. (30) yields the total wave force acting on the structure,

$$f_w(t) = \left\{ \int_0^d \left[K_d \sqrt{\frac{8}{\pi}} \sigma_v T_v + K_m T_a \right] \phi_w(z) dz \right\} \eta(t) \quad (39)$$

where,

$$T_a = -j\omega^2 \frac{\cosh(kz)}{\sinh(kd)}. \quad (40)$$

As the surface elevation of the sea rises and falls, the force is lumped proportionally into the 3 nodes at the low, mean and high water levels, which can be seen in Fig. 1.

5. Joint distribution of wind and waves

The JONSWAP spectrum defined in Section 4 is a stationary Gaussian process, and can be mapped into the process of the sea state defined by (H_s, T_z) by letting the dimensionless time be t/T_z and the dimensionless process be $X/\sqrt{\lambda_0} = 4X/H_s$ [7]. The wind speed at 10 m, U_{10} , and the significant wave height from the JONSWAP spectrum, H_s , can be related through the integral of Eq. (25)

$$\sigma^2 = \int_0^\infty S_{\eta\eta}(\omega) d\omega = \lambda_0 \quad (41)$$

where, σ is the standard deviation of surface displacement. If a sea contains a narrow range of wave frequencies, H_s is related to the standard deviation of the sea surface displacement [47]

$$H_s = 4\sigma. \quad (42)$$

The sample functions used for analysis in the joint distribution of wave period and height are approximated by the trigonometric polynomial [48]

$$X(t) = \sum_{k=1}^n \sqrt{S_{\eta\eta}(\omega_k) d\omega} (X_{1k} \cos \omega_k t + X_{2k} \sin \omega_k t) \quad (43)$$

where X_{1k} and X_{2k} for $k = 1, \dots, n$ are mutually independent standard normal variables and $\omega_{k+1} = \omega_k + d\omega$, with $d\omega$ being an infinitesimal frequency step.

6. Fatigue analysis

The fatigue evaluation applies Miner's law, considering the plate thickness effect and environmental conditions in accordance with [40]. The fatigue curve ($S-N$ chart) that was applied [41] is given by

$$\log_{10} N = \log_{10} a - m \log_{10} \left(\Delta\sigma \left(\frac{t}{t_{ref}} \right)^k \right) \quad (44)$$

where, N is the allowed cycles of the stress range $\Delta\sigma$ (MPa), $\log_{10} a$ is the intercept on the $\log_{10} N$ axis for the $S-N$ curve, m is the coefficient that represents the inclination, t_{ref} is the reference plate thickness, t is the plate thickness, and k is an index parameter.

The degree of fatigue damage is given by

$$D_D = \sum_{i=1}^I \frac{n_{C,i}}{N_{D,i}} \quad (45)$$

and the fatigue life is given by

$$Y = \frac{1}{D_D} \quad (46)$$

where, $n_{C,i}$ is the number of stress cycles in the i th stress block and $N_{D,i}$ is the number of cycles to failure at the design stress range of the i th stress block interpreted from the characteristic long-term distribution of stress ranges.

7. Numerical examples

The time histories and power spectral densities of the wind and wave loadings are presented first. Next, the MDOF offshore structure with and without TLCD is excited by wind loading, followed by combined wind and wave loading. Finally, the MDOF model with rotating blades and TLCD is subjected to a combined wind and wave loading. Fig. 1 shows the structural model under consideration with the corresponding idealized lumped mass MDOF system, with each lumped mass node connected by massless elements having finite stiffness [42]. The foundation is assumed to be fully fixed into the ground, with no rotation allowed. The base of the tower, d_s , is 4.3 m in diameter, tapering to 3.5 m at the nacelle. The steel thickness at the bottom and the top of the structure is 18 mm and 10 mm, respectively. Steel with an elastic modulus equal to 210×10^9 N/m² was assumed to be used in the construction of the turbine. The structural damping ratio is assumed to be 0.01.

7.1. Wind and wave excitations

Sample time histories and the PSDFs for both the wind and the wave excitations are presented in Figs. 2–8. The mean wind velocities used to calculate the forces at the top of the tower in Figs. 2 and 6 were taken as 18 m s⁻¹ and 30 m s⁻¹ respectively. The density of air, the coefficient of drag and the roughness length for the water surface were taken as 1.2 kg/m³, 1.2 and 0.002, respectively. Time histories of duration 50 s are presented. Fig. 2 shows the time history of the drag force for the wind excitation at node 7. Fig. 3 shows the target and simulated PSDFs for the wind spectrum. It can be seen that in both the wind and the wave excitation cases, the target power spectral densities show close agreement with the simulated PSDFs (Figs. 3 and 5).

Two types of wave spectra were used in the analysis, a 'moderate' wave time history and a 'strong' wave time history. The following parameter values were used in the 'moderate' wave spectra simulation: $k_0 = 1$, $l_x = 1200$ m, $C_d = 1.2$, $\rho_0 = 1.2$ kg/m³, $z = 40$ m, $\alpha_p = 0.23$, $U_{10} = 18$ (m/s), $g = 9.81$ m/s/s, $F = 85,000$ m and $\gamma = 3.3$. The resulting time history of the surface elevation of the sea for the 'moderate' wave loading can be seen in Fig. 4. The PSDF for the moderate wave excitation can be seen in Fig. 5. The nodal drag force for the 'moderate' wave excitation at node 3 is presented in Fig. 6.

The following parameter values were used in the 'strong' wave spectra simulation: $k_0 = 1$, $l_x = 1200$ m, $C_d = 1.2$, $\rho_0 = 1.2$ kg/m³ (at sea level with 20 °C dry air), $z = 40$ m, $\alpha_p = 0.23$, $U_{10} = 30$ (m/s), $g = 9.81$ m/s/s, $F = 85,000$ m and $\gamma = 3.3$. The resulting time history of the surface elevation of the sea for the 'strong' wave loading can be seen in Fig. 7. The PSDF for the moderate wave excitation can be seen in Fig. 8. The nodal drag force for the 'moderate' wave excitation at node 3 is presented in Fig. 9.

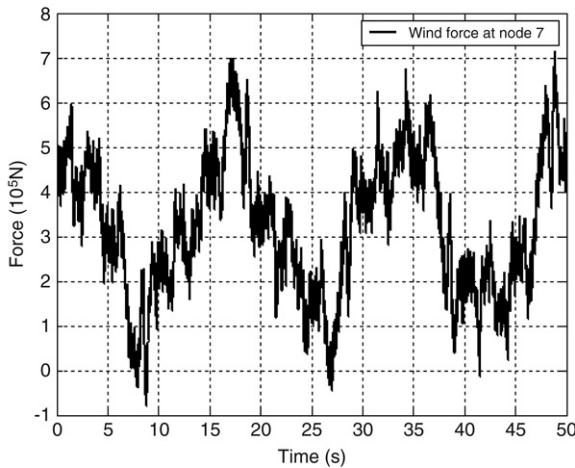


Fig. 2. Time series for wind excitation at Node 7.

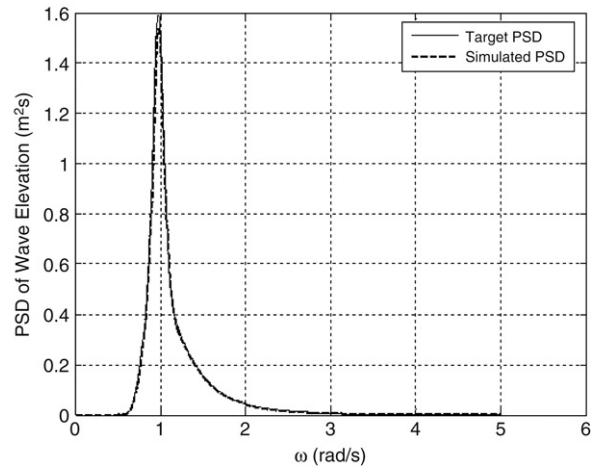


Fig. 5. PSDF of 'moderate' wave elevation.

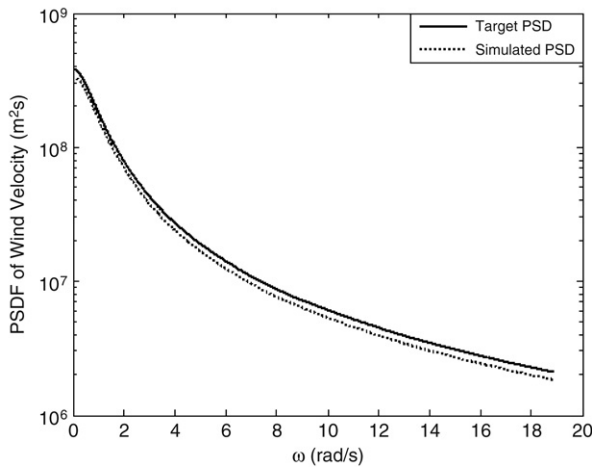


Fig. 3. PSDF for the wind excitation.

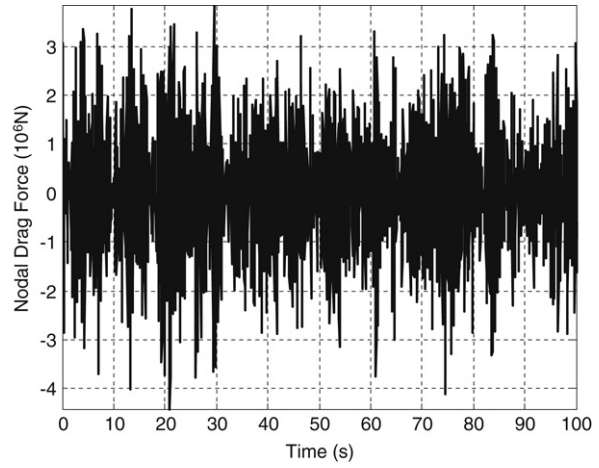


Fig. 6. Wave force at node 3 for 'moderate' wave excitation.

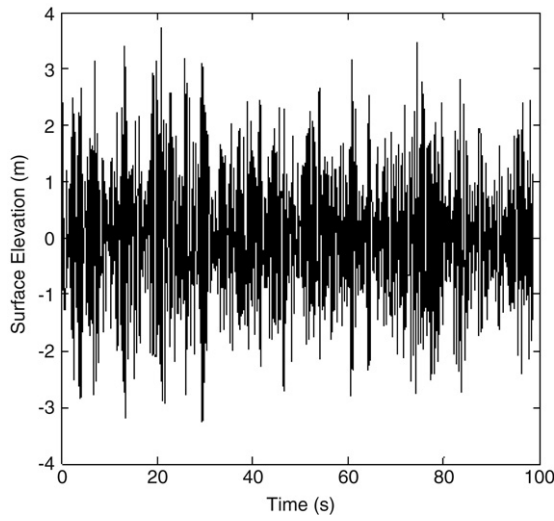


Fig. 4. Time series for the 'moderate' wave excitation.

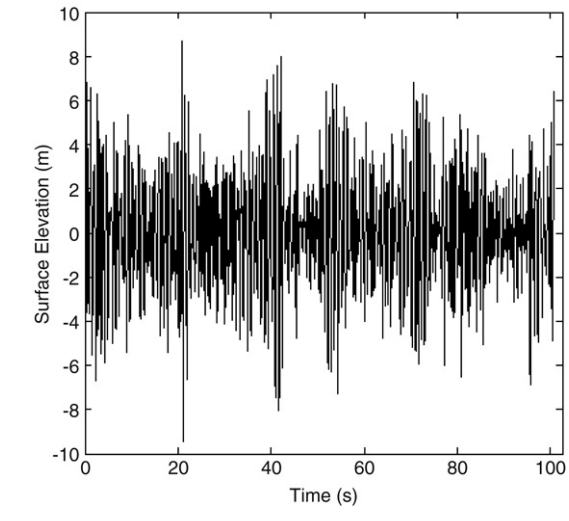


Fig. 7. Time series for the 'strong' wave excitation.

7.2. MDOF tower with blades lumped at nacelle under 'moderate' wind excitation

The structure adopted in the numerical study is an offshore wind turbine of total height 100 m. The turbine tower with the blades lumped at the nacelle is first considered, in order to

investigate the performance of a TLCD on a cantilevered structure subject to wind excitation. The average wind speed used in this section is 30 m/s and the wave force applied at node 7 can be seen in Fig. 2. The fundamental natural frequency of the system, to which most of the peak displacement may be attributed to, for the structure without TLCD is 1.1146 rad/s.

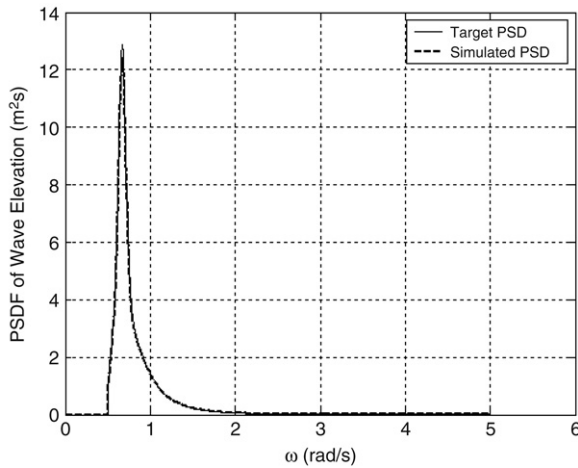


Fig. 8. PSDF of 'strong' wave elevation.

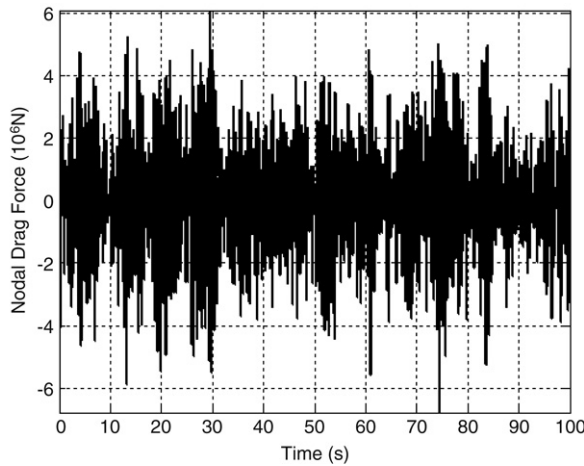


Fig. 9. Wave force at node 3 for 'strong' wave excitation.

The parameters of the TLCD were optimised to impart the highest damping on the structural system [24]. The mass of the TLCD, which was 1% of the total mass of the structure, was 1.6 tonnes. The natural frequency of the TLCD was tuned to 99.2% of that of the fundamental frequency of the MDOF structure. The total length of the liquid column in the TLCD was 15.2 m. The breadth, B , which is the horizontal part of the TLCD, is taken as 2.5 m, leaving vertical columns of 6.35 m. The cross sectional area of such a TLCD is 0.13 m^2 , which equates to sides of the square cross section of 0.36 m. In terms of accommodating the TLCD in an offshore wind turbine, the vertical columns could be located in the tubular tower below the nacelle, or within the tubular tower and through the nacelle, or embracing the interior/exterior surface of the nacelle. In the nacelle a higher horizontal section of the TLCD would be available. The values of ξ and α were 30 and 0.2, respectively. The larger the value of α , which is the ratio of the breadth of the TLCD to that of the length of the liquid column, the more effective the TLCD. However, in the case of a TLCD in a wind turbine, horizontal space is at a premium, so one must use a lower value of α than is ideal in order to tune the TLCD to the natural frequency of the wind turbine.

Fig. 10 shows the mode shapes of the structure. Fig. 11 displays a segment of the time history responses for both the MDOF structure without TLCD and MDOF structure with TLCD in the case of a fluctuating wind of mean 30 m/s. A reduction from the peak displacement of approximately 35.5% is obtained by installing the TLCD in the offshore wind turbine subjected to wind loading and

no wave loading. For the theoretical case under consideration, the peak design bending moment at the base from the contribution of the vibrating tower is reduced from $3.1234 \times 10^5 \text{ kN m}$ to $1.7312 \times 10^5 \text{ kN m}$.

7.3. MDOF tower with blades lumped at the nacelle under 'strong' wind and wave excitation

In this section, the MDOF offshore wind turbine with and without TLCD is excited by a combined wind and wave loading. The wave loading in Fig. 9 is the input wave excitation in this case. As the surface elevation increases and decreases, the total force from the sea is lumped into the appropriate nodes. Fig. 12 presents the time-history response of the MDOF system subjected to a combined wind and wave loading. It can be seen that the interaction of the wind and wave forces increases the peak response of the structure without TLCD by approximately 55% at its peak. In the time segment presented, the influence of the TLCD is evident in reducing the peak response by 38% at approximately 1.1 s. The peak bending moment for the turbine without damper is $4.1356 \times 10^5 \text{ kN m}$ as opposed to $2.49 \times 10^5 \text{ kN m}$ for the turbine with TLCD.

7.4. MDOF tower with rotating blades under 'moderate' wind and wave excitation

The MDOF structure (with and without TLCD) with rotating blades was subjected to a wind and wave loading. The wind velocity taken at height of 10 m was 18 m/s. The blades were 60 m in length and individually weighed 9.5 tonnes. The blades rotated at a frequency equal to the fundamental natural frequency of the MDOF system. The altered fundamental frequency for the tower-blade system is 0.93 rad/s . Thus, the length of the liquid column is 22.6 m, and the value of α is 0.11. The time history response of the aforementioned system is given in Fig. 13.

It can be seen that in times of moderate wind and wave loading, the blades impart the largest loading on the structural tower. The response of the tower with TLCD shows a marked reduction when a TLCD is employed, with reductions of approximately 60% in the response evident. The maximum design bending moment for the theoretical simulation at the base of the structure from is reduced from $6.2607 \times 10^4 \text{ kN m}$ to $4.0101 \times 10^4 \text{ kN m}$.

7.5. MDOF tower with rotating blades under 'strong' wind and wave excitation

Next, the MDOF (with and without TLCD) structure with rotating blades was subjected to a stronger wind and wave loading. The applied wind and wave loadings in this case can be seen in Figs. 2 and 6 respectively. The time history response of the aforementioned system is given in Fig. 14.

For the MDOF system with optimised TLCD, a maximum reduction of 55% is recorded as compared to that of the MDOF system without TLCD. The maximum design bending moment for the theoretical simulation at the base of the structure from is reduced from $5.35 \times 10^5 \text{ kN m}$ to $2.99 \times 10^5 \text{ kN m}$. The variation of the base moment for the aforementioned numerical case is presented in Fig. 15.

8. Fatigue life

This study calculates the fatigue life of the turbine tower with and without the TLCD, using the rain-flow calculation method. The tower locations chosen for the fatigue analysis are the butt weld

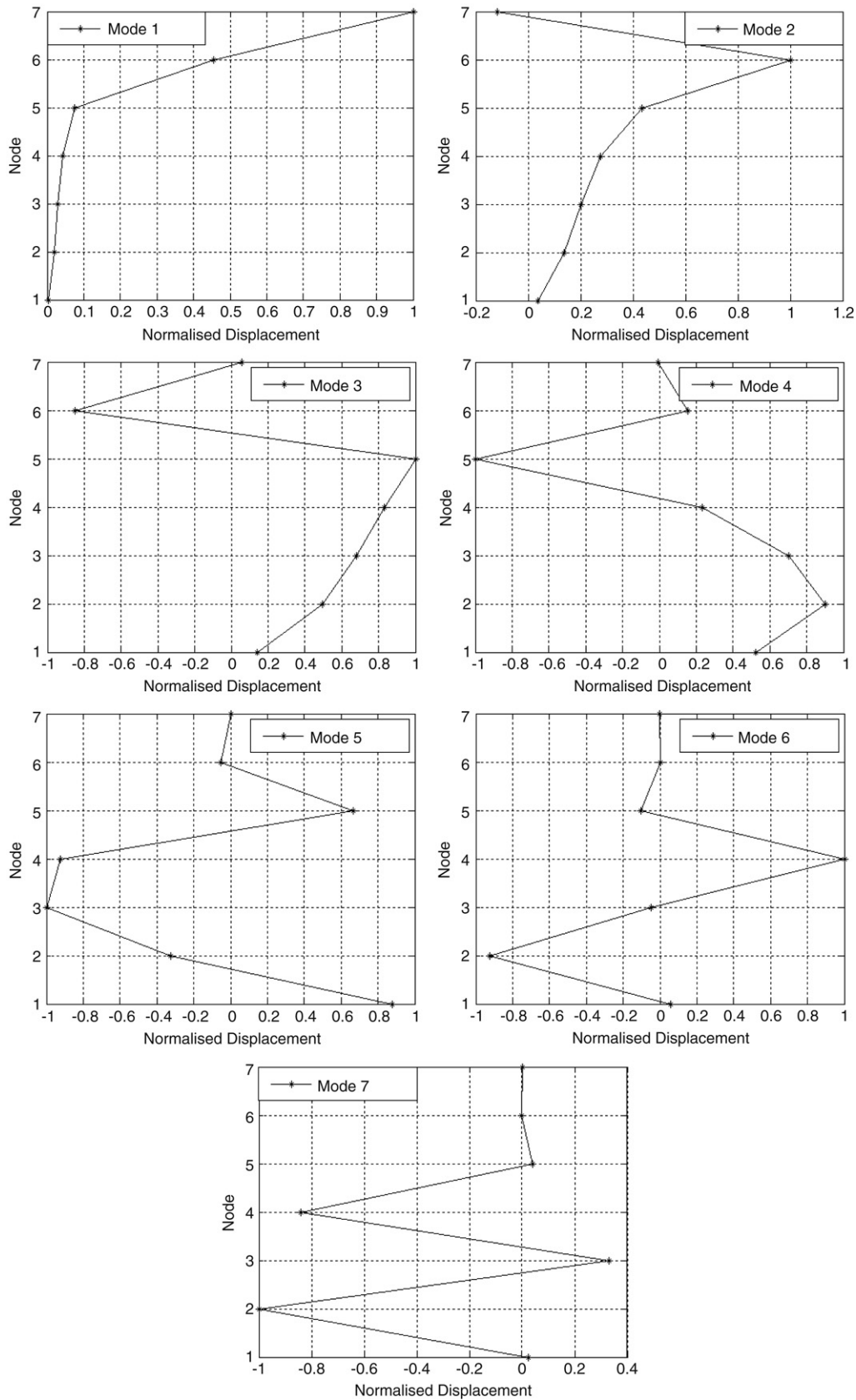


Fig. 10. Mode shapes of MDOF system.

connection connecting the tower to the mono-pile foundation (which in this case is taken as 1 m below the platform mass, fatigue analysis point 1 in Fig. 1) and the connection of the mono-pile

foundation with the sea-bed (which is taken as 1 m above the point of fixity, fatigue analysis point 2 in Fig. 1). The following specific set values are taken from [41].

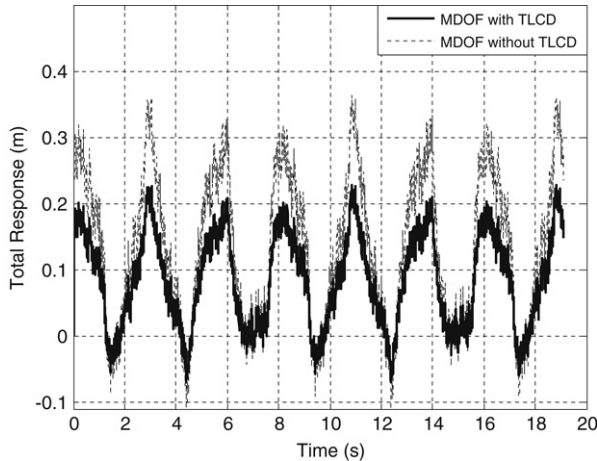


Fig. 11. MDOF time-history response under wind excitation with and without TLCD.

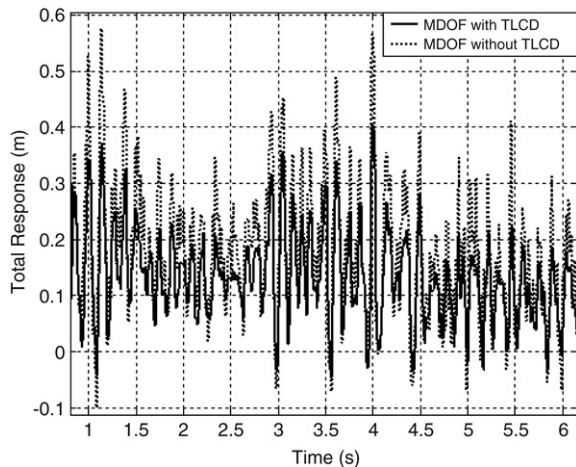


Fig. 12. MDOF time-history response under wind and wave excitation with and without TLCD.

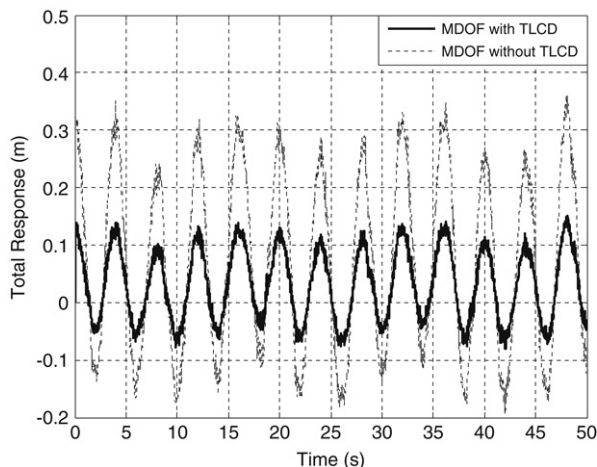


Fig. 13. MDOF, with rotating blades, time-history response under 'moderate' wind and wave excitation with and without TLCD.

- (a) Conditions in the atmosphere
 - $\log_{10} a = 12.164, m = 3, k = 0.20 (N < 10^7)$.
- (b) Undersea conditions (with electrolytic protection)
 - $\log_{10} a = 11.764, m = 3\gamma, k = 0.20, \gamma$ (material coefficient) = 1.25 ($N < 10^7$).

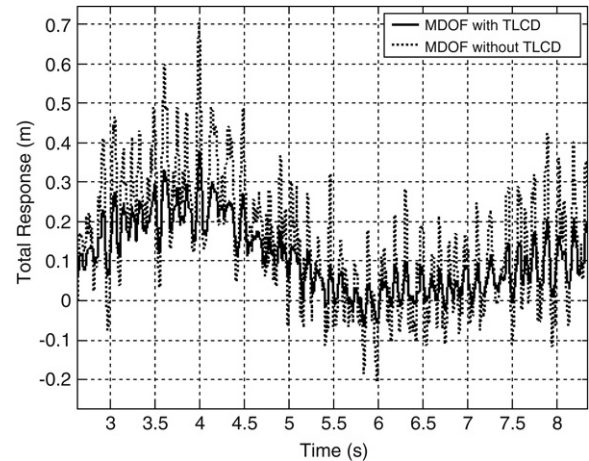


Fig. 14. MDOF, with rotating blades, time-history response under 'strong' wind and wave excitation with and without TLCD.

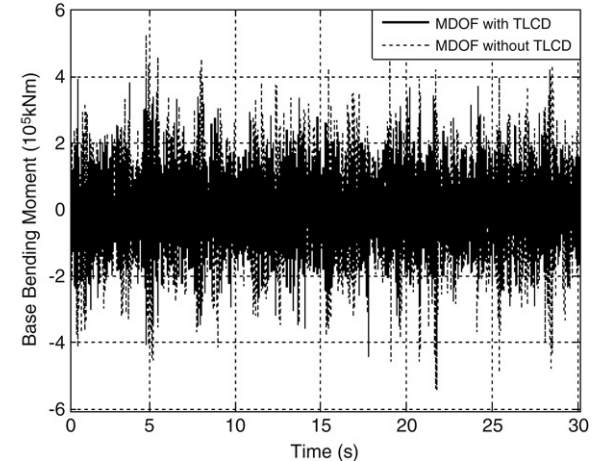


Fig. 15. Base bending moment of MDOF, with rotating blades, time-history response under 'strong' wind and wave excitation with and without TLCD.

Table 1 presents the cumulative fatigue damage rate and fatigue life obtained by the rain-flow calculation method. The results of the fatigue life calculations indicate that the life span of a wind turbine assembly with TLCD is substantially longer than that of a wind turbine assembly without TLCD.

9. Conclusions

This paper examined the excitation of an offshore wind turbine modelled as a MDOF system under wind and wave loadings. The Kaimal spectrum was chosen to represent the wind excitation, and the JONSWAP spectrum was used for the wave excitation. Cases of the blades lumped at the nacelle and of rotating blades were separately examined. It was found that when an offshore wind turbine is equipped with a TLCD and subjected to wind and wave forces, reductions of up to 55% in the peak response of the same system without TLCD may be achieved. This leaves the option open to design the wind turbine more efficiently, with less steelwork and lower foundation expenses. It was also observed that implementation of a damper such as a TLCD in an offshore wind turbine greatly increases the fatigue life of the wind tower assembly. In spite of the provision of a low ratio of horizontal to the total length of TLCD in a wind turbine, the numerical study carried out in this paper has shown that even a TLCD designed with low 'efficiency', can suppress vibration considerably for the cases considered. However, in view of the restriction in the provision of

Table 1

Degree of fatigue damage for wind turbine assembly with and without TLCD

Location	Case	Cumulative fatigue damage rate (year)	Fatigue life (years)
Mono-pile foundation top	Tower without TLCD	0.00117	895
	Tower with TLCD	0.00014	3192
Mono-pile foundation seabed	Tower without TLCD	0.012192	82
	Tower with TLCD	0.000906	390

the available ‘horizontal length’ for a TLCD in a wind turbine other dampers such as TMDs and TLDs may prove to be more efficient in certain cases, and case specific studies should be carried out to choose the best option.

References

- [1] Hasselmann K, Barnett TP, Bouws E, Carlson H, Cartwright DE, Enke K, et al. Measurement of wind-wave growth and swell decay during the joint north sea wave project (JONSWAP). *Deutsche Hydrogr* 1973;Z.A8(12).
- [2] Pierson WJ, Moskowitz L. A proposed spectral filter for fully-developed wind seas based on the similarity theory of S.A. Kitaigorodski. *J Geophys Res* 1964; 69:5181–203.
- [3] Davenport AG. The spectrum of horizontal gustiness near the ground in high winds. *J R Meteorological Soc* 1961;87:194–211.
- [4] Harris RI. The nature of wind, in the modern design of wind sensitive structures. London (Great Britain): Construction Industry Research and Information Association; 1971.
- [5] Harris RI. Some further thoughts on the spectrum of gustiness in strong winds. *J Wind Eng Ind Aerodyn* 1990;33:461–7.
- [6] Kaimal JC, Wyngaard JC, Izumi Y, Cote OR. Spectral characteristics of surface-layer turbulence. *J R Meteorological Soc* 1972;98:563–89.
- [7] Ditlevsen O. Stochastic model for joint wind and wave loads on offshore structures. *Struct Safety* 2002;24:139–63.
- [8] Stewart RH. Introduction to physical oceanography. Texas A&M University; 2005.
- [9] Hasselmann DE, Dunckel M, Ewing JA. Directional wave spectra observed during JONSWAP 1973. *J Phys Oceanogr* 1980;10(8):1264–80.
- [10] Morison JR, et al. The forces exerted by surface waves on piles. *Pet Trans, AIME* 1950;189:149–54.
- [11] Lee HH. Stochastic analysis for offshore structures with added mechanical dampers. *Ocean Eng* 1997;24(9):817–34.
- [12] Li HJ, Hu SJ. Tuned mass damper design for optimally minimizing fatigue damage. *J Eng Mech* 2002;128(6):703–7.
- [13] Li JL, Hu SJ, Jakubiak C. H2 active vibration control for offshore platform subjected to wave loading. *J Sound Vib* 2003;263:709–24.
- [14] Ma H, Tang GY, Zhao CD. Feedforward and feedback optimal control for offshore structures subjected to irregular wave forces. *Ocean Eng* 2006;33: 1105–17.
- [15] Ahmad SK, Ahmad S. Active control of non-linearly coupled TLP response under wind and wave environments. *Comput Struct* 1999;72:735–47.
- [16] Sakai F, Takaeda S, Tamaki T. Tuned liquid column damper- new type device for suppression of building vibrations. In: Proceedings of international conference on highrise buildings. 1989, p. 926–31.
- [17] Shimizu K, Teramura A. Development of vibration control system using U-shaped tank. In: Proceedings of the 1st international workshop and seminar on behavior of steel structures in seismic areas. 1994.
- [18] Vandiver JK, Mitone S. The effect of liquid storage tanks on the dynamic response of offshore platforms. In: Dynamic analysis of offshore structures: Recent developments. 1978.
- [19] Samali B, Lee P, Kwok KCS. Wind-induced vibration control of tall buildings with tuned liquid column dampers. In: Proceedings of the 1st international conference on motion and vibration control. 1992, p. 182–7.
- [20] Xu YL, Samali B, Kwok KCS. Control of along-wind response of structures by mass and liquid dampers. *J Eng Mech* 1992;118(1):20–39.
- [21] Hochrainer MJ. Control of vibrations of civil engineering structures with special emphasis on tall buildings. Austria: Vienna University of Technology; 2001.
- [22] Balendra T, Wang CM, Cheong HF. Effectiveness of tuned liquid column dampers for vibration control of structures. *Eng Struct* 1995;17(9):668–75.
- [23] Balendra T, Wang CM, Rakesh G. Vibration control of tapered buildings using TLCD. *J Wind Eng Ind Aerodyn* 1998;77–78(1–2):245–57.
- [24] Gao HK, Kwok CS, Samali B. Optimization of tuned liquid column dampers. *Eng Struct* 1997;19(6):476–86.
- [25] Hochrainer MJ, Ziegler F. Control of tall building vibrations by sealed tuned liquid column dampers. *Struct Control Health Monit* 2006;13(6): 980–1002.
- [26] Ziegler F. The tuned liquid column damper as the cost-effective alternative of the mechanical damper in civil engineering structures. *Int J Acoustics Vib* 2007;12(1):25–39.
- [27] Ghosh A, Basu B. Seismic vibration control of nonlinear structures by LCD. *J Struct Eng ASCE* 2008;134(1):146–53.
- [28] Ghosh A, Basu B. Seismic vibration control of short period structures using the liquid column damper. *Eng Struct* 2004;26(16):1905–13.
- [29] Shum KM, Xu YL. Multiple-tuned liquid column dampers for torsional vibration control of structures: Experimental investigation. *Earthq Eng Struct Dyn* 2002;31:977–91.
- [30] Xue SD, Ko JM, Xu YL. Tuned liquid column damper for suppressing pitching motion of structures. *Eng Struct* 2000;23:1538–51.
- [31] Wu JS, Hsieh M. Study on the dynamic characteristic of a U-type tuned liquid damper. *Ocean Eng* 2002;29:689–709.
- [32] Colwell S, Basu B. Investigations on the performance of a liquid column damper (LCD) with different orifice diameter ratios. *Can J Civil Eng* 2006;33(5): 588–595.
- [33] Colwell S, Basu B. Experimental and theoretical investigation on equivalent viscous damping of structures with TLCD for different fluids. *J Struct Eng ASCE* 2008;134(1):154–63.
- [34] Hochrainer MJ, Adam C, Ziegler F. Application of tuned liquid column dampers for passive structural control. In: Proc 7th international congress of sound and vibrations. Germany: Garmisch-Partenkirchen; 2000.
- [35] Hochrainer MJ, Ziegler F. Tuned liquid column damper – a cheap device for control of tall building vibrations. In: Flesch R, Irschik H, Krommer M, editors. 3rd European conference on structural control. Schriftenreihe der TU-Wien; 2005, p. S1–179–S1–182.
- [36] Ziegler F. Sealed tuned liquid column dampers make high-rise buildings smart. In: Sabouni A-RR, El-Sawy KM, editors. 7th International conference on multi-purpose high-rise towers and tall buildings. Dubai: The International Federation of High-Rise Structures; 2005, p. 1–17.
- [37] Brughuis FJ, Wilminck AJ. Damping of Wind Turbine, www.espacenet.com, 2006. E.P. Office, Editor. Netherlands.
- [38] Colwell S, Basu B. Tuned liquid column dampers in offshore wind turbines. In: Proceedings of the 5th world wind energy conference. 2006.
- [39] Colwell S, Basu B. Vibration control of an offshore wind turbine with a tuned liquid column damper. In: Topping BHV, editor. Proceedings of the eleventh international conference on civil, structural and environmental engineering computing. Malta, CD ROM: Civil-Comp Press; 2007.
- [40] DNV, Design of offshore wind turbine structures. Offshore Standard DNV-OS-J101, 2004.
- [41] Shiraishi S, et al. Experimental fatigue analysis of an offshore wind power generation facility. In: World wind energy conference 2007. 2006.
- [42] Rogers N. Structural dynamics of offshore wind turbines subject to extreme wave loading. In: Proceedings of the 20th BWRA annual conference. 1998.
- [43] Simiu E, Scanlan RH. Wind effects on structures: An introduction to wind engineering. Wiley-Interscience; 1978.
- [44] Murtagh PJ. Ph. D. dissertation: Dynamic response of wind turbine tower assemblies. Department of Civil, Structural & Environmental Engineering, Trinity College Dublin; 2005.
- [45] Murtagh PJ, Basu B, Broderick BM. Along-wind response of a wind turbine tower with blade coupling subjected to rotationally sampled wind loading. *Eng Struct* 2005;27:1209–19.
- [46] Sarpkaya T, Isaacson M. In: Reinholt VN, editor. Mechanics of wave forces on offshore structures. 1981, New York.
- [47] Hoffman DaK, OJ. The theory of Rayleigh distribution and some of its applications. *J Ship Res* 1975;19(3):172–91.
- [48] Colwell S, Basu B. Simulation of joint wind and wave loading time histories. In: Proceedings of the Irish signals and systems conference. 2006, paper no 120.